Analysis and Design of Load-Independent Series Resonant Power Amplifier With Constant Current Output and Its Application for WPT System

Yutaro Komiyama, *Graduate Student Member, IEEE*, Ayano Komanaka, Wenqi Zhu, *Member, IEEE*, Akihiro Konishi, *Member, IEEE*, Kien Nguyen, *Senior Member, IEEE*, and Hiroo Sekiya, *Senior Member, IEEE*

***Abstract*—This article presents an analysis and design of a load-independent (LI) series resonant (SR) power amplifier with constant current (CC) output, along with its application for an MHz wireless power transfer (WPT) system. A novel inverse Class E power amplifier is introduced, which essentially produces a sinusoidal output current even with a low-Q SR filter. Besides, the proposed amplifier achieves zero-current switching and CC output simultaneously, regardless of the load resistance. The LI operation is obtained for a specific set of component values, whose design conditions are clarified analytically in this article. The experiment was carried out with a WPT system incorporating the proposed amplifier as a transmitter and the Class D rectifier as a receiver. Although the input reactance of the Class D rectifier changed against dc-load variations due to the parasitic capacitances, the proposed amplifier showed consistent CC operation by using the low-Q SR filter. Also, the proposed WPT system maintained a low total harmonic distortion of the transmission current over the wide load range, even with the low-Q output filter. The prototype WPT system with the proposed amplifier achieved 88% power-delivery efficiency with 60 W output power at 3.39 MHz transmission frequency. The experimental results showed the effectiveness of the proposed amplifier.**

***Index Terms*—Constant current (CC), inverse class e amplifier, load-independent (LI), total harmonic distortion (THD), wireless power transfer (WPT).**

I. Introduction

HIGH performance power semiconductor devices, such as gallium nitride (GaN) and silicon carbide devices, have enabled the high-frequency and high-efficiency operation of power amplifiers [1], [2], [3]. The power amplifiers at the megahertz frequency band are explored and developed, reducing the size and weight of the passive components. Meanwhile, high-frequency operation brings challenges, including growing switching losses and difficulty in high-side gate drives. Thus, the Class E amplifier family, including Class E [1], [2], [3], [4], [5], [6], [7], [8], [9], [10], [11], [12], [13], [14], Class EF [15], [16], [17], and Class Φ amplifiers [18], [19], have attracted attention due to its simple configuration and soft switching feasibility. However, the Class E amplifiers are essentially sensitive against load variations [5], [6]. The load variations change the circuit operation drastically, causing output voltage variations and efficiency degradation due to hard switching.

To overcome the sensitivity, a load-independentss E amplifier was proposed [7], which enhances the robustness against load variations. The LI Class E amplifier uses a finite input coil, which works as a resonant inductance. Namely, the LI Class E amplifier expands the design flexibility to obtain robustness by introducing a new resonant structure. The LI Class E amplifier maintains soft switching against load variations. In addition, the amplitude of the output ac voltage is constant regardless of the load resistance. The robustness can be obtained by a specific tuning of component values without additional controls [8] and circuitry [9]. The design technique of the LI Class E amplifier has also been applied to various circuit topologies in the Class E amplifier family [11], [12], [13], [14], [15], [16], [17], [18], [19], [20], [21]. Depending on the circuit topology, the LI amplifiers inherently exhibit different characteristics in output types, constant current (CC) or constant voltage, soft switching [zero-voltage switching (ZVS) or zero-current switching (ZCS)], and output-resonant filters [series resonant (SR) or parallel resonant (PR)]. Accordingly, the LI amplifiers can be adapted to a wide range of applications and specifications, such as dc–dc converters [13] and the transmitter of wireless power transfer (WPT) systems [15], [16], [17]. Especially for WPT applications, the CC output amplifier with the SR output filter is preferable. This is because it avoids overcurrents flowing through the transmitter coil even when the receiver circuit moves away.

Owing to the CC-SR feature, the LI Class EF amplifier has proven successful in applications as a transmitter for WPT systems [15], [16], [17]. In addition, the Class EF amplifier mitigates switch–voltage stress by adding a harmonic resonant branch. In the original Classes EF_2 and E/F_3 amplifiers [22], [23], [24], the harmonic resonant filter is tuned to an integer

Manuscript received 14 November 2023; revised 28 January 2024; accepted 6 February 2024. Date of publication 20 February 2024; date of current version 20 March 2024. This work was supported in part by the Commissioned Research Project under Grant JPJ012368C07001, and in part by the National Institute of Information and Communications Technology (NICT), Japan. Recommended for publication by Associate Editor Dongyuan Qiu. *(Corresponding author: Hiroo Sekiya.)*

The authors are with the Graduate School of Science and Engineering, Chiba University, Chiba 2638522, Japan (e-mail: y.komiyama@chiba-u.jp; sekiya@faculty.chiba-u.jp).

Color versions of one or more figures in this article are available at https://doi.org/10.1109/TPEL.2024.3367373.

Digital Object Identifier 10.1109/TPEL.2024.3367373

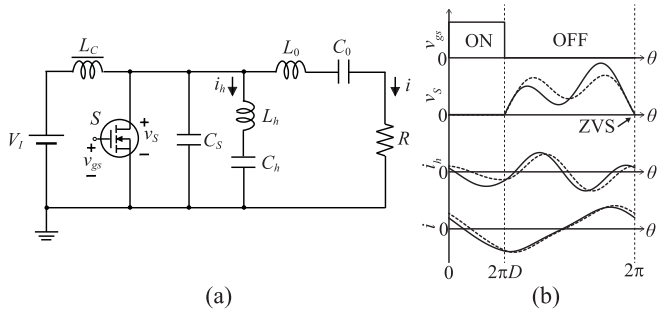

Fig. 1. LI Class EF amplifier. (a) Circuit topology. (b) Example waveforms at fixed load resistances (solid line: $R/R_r = 1$ and dashed line: $R/R_r = 0.1$).

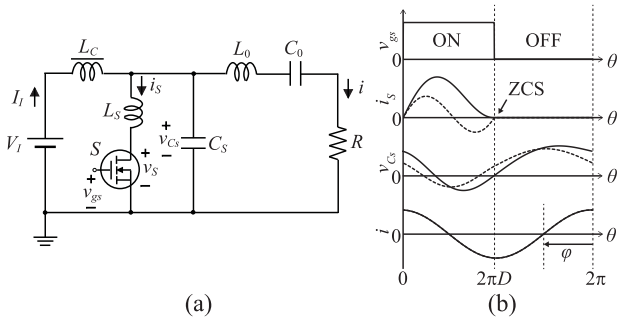

Fig. 2. Proposed amplifier. (a) Circuit topology. (b) Example waveforms for fixed load resistances (solid line: $R/R_r = 1$ and dashed line: $R/R_r = 0.1$).

multiple of the switching frequency. On the other hand, the LI Class EF amplifier employs a resonant frequency approximately 1.7 times the switching frequency [15]. This design, however, leads to significant harmonic distortion in the output current because the harmonic resonant branch cannot fully filter out the harmonics [25]. The high total harmonic distortion (THD) of the current degrades electromagnetic interference performance [26] and efficiency [27]. Furthermore, the harmonics in the output current deteriorate the consistency of the CC operation. Therefore, it is important to develop another CC-SR amplifier topology with a low-THD output current.

This article presents an analysis and design of the LI-SR amplifier with CC output. A novel circuit topology with CC-SR property is introduced, which can inherently output sinusoidal current even with a low-Q SR filter. Analytical design equations of the proposed amplifier are provided, which allows a quick and intuitive component-value selection. This article also presents the design procedure and experiment for the WPT system incorporating the proposed amplifier as the transmitter. The experimental verifications were conducted with the WPT system with the proposed amplifier. The proposed amplifier achieved superior consistency of the CC operation and a lower THD transmission current compared with the LI Class EF amplifier. Furthermore, the proposed amplifier showed low sensitivity to reactance components because it can produce sufficiently pure sinusoidal wave even with the low-Q SR filter. The experimental results showed the validity of the amplifier design and analysis.

II. LI Amplifier With CC-SR Property

This section provides a brief review of the LI Class EF amplifier [15] and introduces the proposed amplifier. These amplifiers have a common feature in the CC-SR property.

A. LI Class EF Amplifier

Fig. 1(a) and (b) shows the circuit topology and example waveforms of the LI Class EF amplifier, respectively, where D is the on-duty ratio, $\theta = \omega t = 2\pi f t$ is the angular displacement, ω denotes the angular switching frequency, and f is the switching frequency. Besides, the subscript "r" of the symbol means its rated value.

The LI Class EF amplifier achieves ZVS and a constant amplitude output current simultaneously, regardless of the load resistance R, as shown in Fig. 1(b). The LI operation is obtained for a specific set of component values, which is determined by satisfying the design conditions of [15]

$$\frac{dI_m}{dR} = 0 \tag{1}$$

and

$$v_S(2\pi D) = 0 \tag{2}$$

where I_m is the amplitude of the output current i. The condition (1) represents the CC operating condition, and (2) shows the ZVS condition. By satisfying (1) and (2) simultaneously, the design parameters for the LI operation are derived. Therefore, the Class EF amplifier only requires specific tuning to obtain robustness against load variations without requiring additional controls and circuits.

However, the LI Class EF amplifier introduces significant harmonic distortion into the output current. This is because the resonant frequency of L_h-C_h needs to be tuned to approximately 1.7 times the switching frequency, and thus, the harmonic current cannot be fully filtered out by L_h-C_h.

Although the harmonics in the output current can be reduced by using a high-Q SR filter, it results in higher sensitivity, a large inductance, and increased voltage stress and power losses for the resonant components. Also, the push–pull topology is effective for suppressing second-order harmonics. It has a tradeoff against the increase in device and component numbers and accurate tuning for circuit balance.

B. Proposed Amplifier

Fig. 2(a) shows the circuit topology of the proposed amplifier, which consists of the dc-input voltage source V_I, choke inductance L_C, series inductance L_S, switching device S, shunt capacitance C_S, SR filter L_0-C_0, and load resistance R. Fig. 2(b) depicts the example waveforms of the proposed amplifier for fixed load resistances.

The choke inductance L_C sufficiently reduces the ripple current and behaves as a dc-current source. The switching device turns ON and OFFperiodically. During the turn-ON period, current flows into the switching device, which achieves ZCS at the turn-OFF moment, as shown in Fig. 2(b). The ZCS is a dual operation of the ZVS in the Class E amplifiers [28]. Namely, the proposed amplifier can be called LI inverse Class E amplifier. The L_S and C_S resonate at slightly higher than the switching

frequency, and the nearly sinusoid voltage appears across the capacitor C_S. The output voltage is generated by extracting a fundamental frequency component from the voltage across C_S through the SR output filter.

The proposed amplifier exhibits robustness against resistive load variations. Namely, the ZCS is maintained regardless of the load resistance, resulting in high-efficiency operation over the wide load range. Also, the amplitude and phase shift of the output current is independent of the load resistance. The output currents for $R/R_r = 1$ and $R/R_r = 0.1$ are completely overlapped in Fig. 2(b).

The proposed amplifier no longer requires a high-Q SR filter because v_{C_S} exhibits inherently close to the sinusoidal waveform. Also, a sufficiently pure sinusoidal output can be obtained even without the SR filter. In the design without the SR filter, C_0 only works as a dc blocking with a large capacitance, while L_0 works as the phase-shift inductance required for the LI design. One major advantage of applying the low-Q SR filter is that the proposed amplifier obtains robustness against reactance component variations.

III. Analysis of Proposed Amplifier

This article provides the waveform expressions, amplifier characteristics, and design equations of the proposed amplifier. The analysis is conducted under the following assumptions.

1) The choke inductance L_C is large enough so that the input current I_I can be regarded as dc.
2) The switching device operates ideally. Namely, the switching time, parasitic capacitances, ONresistance, and threshold voltage are zero, and OFFresistance is infinite. Besides, the switch turns ON during $0 \le \theta < 2\pi D$, and turns OFFduring $2\pi D \le \theta < 2\pi$.
3) The resonant inductance L_0 is devided into a resonant component L_a and an extra-inductive component L_b. The L_a and C_0 resonate at the switching frequency, namely
$$\frac{1}{\omega\sqrt{L_a C_0}} = 1. \tag{3}$$
In addition, the quality factor of the SR output filter $Q = \omega L_0/R$ is high enough so that the output current can be regarded as a pure sine wave as
$$i(\theta) = I_m \sin(\theta + \varphi) \tag{4}$$
where φ is the phase shift from gate-drive voltage defined, as shown in Fig. 2(b), and I_m is the amplitude of the output current.
4) All the passive component works linearly with no parasitic components.

In the analysis, the dimensionless circuit parameters are used to provide a generalized discussion. The voltage and current are normalized by input voltage V_I and rated load resistance R_r, as like
$$v^* = \frac{v}{V_I}, \quad \text{and} \quad i^* = \frac{R_r i}{V_I}. \tag{5}$$
Besides, the component parameters are also normalized by ω and R_r, as like
$$\lambda_S = \frac{\omega L_S}{R_r}, \quad \gamma_S = \frac{1}{\omega C_S R_r}, \quad \text{and} \quad \rho = \frac{R}{R_r}. \tag{6}$$

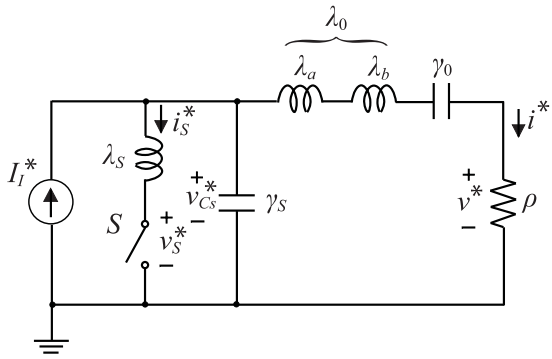

Fig. 3. Analytical model of the proposed amplifier.

Fig. 3 shows the analytical model of the proposed amplifier.

A. Waveform Derivaration

During the switch turn-ON period of $0 \le \theta < 2\pi D$, a second-order differential equation for switch current i_S^* is obtained using KCL as
$$\frac{d^2 i_S^*(\theta)}{d\theta^2} + {\omega_S^*}^2 i_S^*(\theta) = {\omega_S^*}^2 [I_I^* - I_m^* \sin(\theta + \varphi)] \tag{7}$$
where I_I^* is the normalized input current and ω_S^* is defined as
$$\omega_S^* = \sqrt{\frac{\gamma_S}{\lambda_S}}. \tag{8}$$
By solving (7), the switch current for $0 \le \theta < 2\pi D$ can be obtained as
$$i_S^*(\theta) = A\cos(\omega_S^*\theta) + B\sin(\omega_S^*\theta) - \frac{{\omega_S^*}^2 I_m^*}{{\omega_S^*}^2 - 1}\sin(\theta + \varphi) + I_I^*, \quad \text{for } 0 \le \theta < 2\pi D \tag{9}$$
where A and B are constants. Besides, the voltage across γ_S is derived by integrating the current flowing through it as
$$\begin{aligned} v_{C_S}^*(\theta) &= \gamma_S^* \int_0^\theta I_I^* - i_S^*(\theta') - I_m^* \sin(\theta' + \varphi) d\theta' \\ &= -\lambda_S \omega_S^* \left[A\sin(\omega_S^*\theta) - B\cos(\omega_S^*\theta) + \frac{\omega_S^* I_m^*}{{\omega_S^*}^2 - 1}\cos(\theta + \varphi) \right], \quad \text{for } 0 \le \theta < 2\pi D. \end{aligned} \tag{10}$$
During the switch turn-OFF period of $2\pi D \le \theta < 2\pi$, the switch current becomes zero, namely
$$i_S^*(\theta) = 0, \quad \text{for } 2\pi D \le \theta < 2\pi. \tag{11}$$
The expression of the voltage across shunt capacitance during the turn-OFF period, which is the same as the switch voltage, can be given by integrating the current flowing through γ_S as
$$\begin{aligned} & v_{C_S}^*(\theta) \\ &= v_S^*(\theta) = \gamma_S \int_{2\pi D}^\theta I_I^* - I_m^* \sin(\theta' + \varphi) d\theta' \\ &= \gamma_S \{ I_I^*(\theta - 2\pi D) + I_m^* [\cos(\theta + \varphi) - \cos(2\pi D + \varphi)] \} \end{aligned}$$

$$- \lambda_S \omega_S^* \left[A \sin(2\pi D \omega_S^*) - B \cos(2\pi D \omega_S^*) + \frac{\omega_S^* I_m^*}{{\omega_S^*}^2 - 1} \cos(2\pi D + \varphi) \right], \quad \text{for } 2\pi D \le \theta < 2\pi. \tag{12}$$

Note that the boundary condition at $\theta = 2\pi D$ with (10) is taken into account in (12).

B. Boundary Condition

From the continuity of the current flowing through λ_S and the voltage across γ_S, we obtain the boundary conditions as

$$i_S^*(0) = i_S^*(2\pi) \tag{13}$$

and

$$v_{C_S}^*(0) = v_{C_S}^*(2\pi). \tag{14}$$

From (9)–(14), the constants A and B can be obtained as

$$A = \frac{{\omega_S^*}^2 I_m^*}{{\omega_S^*}^2 - 1} \sin\varphi - I_I^* \tag{15}$$

and

$$B = \left\{ \frac{\omega_S^* [\cos(2\pi D \omega_S^*) - (1 - 2{\omega_S^*}^2)\cos\varphi]}{({\omega_S^*}^2 - 1)[1 - \cos(2\pi D \omega_S^*)]} - \frac{{\omega_S^*}^2 \sin\varphi \sin(2\pi D \omega_S^*)}{({\omega_S^*}^2 - 1)[1 - \cos(2\pi D \omega_S^*)]} \right\} I_m^* + \frac{\pi \omega_S^* + \sin(2\pi D \omega_S^*)}{1 - \cos(2\pi D \omega_S^*)} I_I^*. \tag{16}$$

C. LI Condition

The proposed amplifier achieves ZCS at the turn-OFF instant, namely

$$i_S^*(2\pi D) = 0. \tag{17}$$

There is no power loss factor in this analysis. Therefore, the input and output powers are equal. Hence, we have

$$1 \times I_I^* = \frac{\rho {I_m^*}^2}{2}. \tag{18}$$

From (9), (17), and (18), the relationship between I_m^* and ρ is obtained as

$$[\pi(1-D)\omega_S^* \sin(2\pi D \omega_S^*) + 1 - \cos(2\pi D \omega_S^*)] I_m^* \rho - \frac{4{\omega_S^*}^2 \sin(\pi D + \varphi) \sin(\pi D \omega_S^*) \sin[\pi D(1 - \omega_S^*)]}{{\omega_S^*}^2 - 1} = 0. \tag{19}$$

For achieving the CC output, I_m^* must be independent from ρ. This means that the coefficient of ρ and the constant term in (19) must be both zero. Thus, we have the LI-design conditions as

$$\pi(1-D)\omega_S^* \sin(2\pi D \omega_S^*) + 1 - \cos(2\pi D \omega_S^*) = 0 \tag{20}$$

and

$$\varphi = \pi(1 - D). \tag{21}$$

By satisfying (20) and (21), the proposed amplifier attains the ZCS and CC output regardless of the load resistance. Fig. 4 shows the normalized resonant angular frequency ω_S^* and phase shift φ that satisfy (20) and (21).

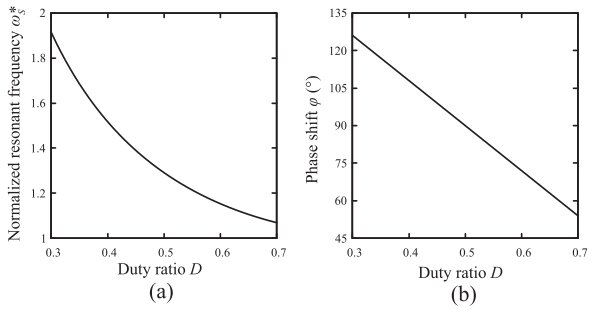

Fig. 4. Circuit parameters that satisfy the LI conditions as functions of duty ratio D. (a) Normalized resonant angular frequency ω_S^*. (b) Phase shift between output current and gate-drive voltage.

D. SR Output Filter

From the assumption, the SR output filter $\lambda_0 - \gamma_0$ passes only a fundamental frequency component from the voltage across γ_S. Namely, we obtain

$$v_{C_{S1}}^*(\theta) = \rho I_m^* \sin(\theta + \varphi) + \lambda_b I_m^* \cos(\theta + \varphi) \tag{22}$$

where $v_{C_{S1}}^*$ is the fundamental frequency component in $v_{C_S}^*$. By applying the Fourier Series EXPANSION for (22) and considering (20) and (21), we obtain

$$\rho I_m^* = \frac{1}{\pi} \int_0^{2\pi} v_{C_S}^*(\theta) \sin(\theta + \varphi) d\theta = \frac{2\gamma_S {\omega_S^*}^2 [\pi(1-D)\cos(\pi D) + \sin(\pi D)]}{\pi({\omega_S^*}^2 - 1)} I_I^* \tag{23}$$

and

$$\lambda_b I_m^* = \frac{1}{\pi} \int_0^{2\pi} v_{C_S}^*(\theta) \cos(\theta + \varphi) d\theta = \frac{\gamma_S {\omega_S^*}^2}{\pi({\omega_S^*}^2 - 1)} \left\{ \pi(1-D) + \frac{\sin(\pi D)}{2} - \frac{\pi}{{\omega_S^*}^2} + \frac{2\sin(\pi D)[\sin(\pi D) + \pi(1-D)\cos(\pi D)]}{\pi(1-D)({\omega_S^*}^2 - 1)} \right\} I_m^*. \tag{24}$$

E. Amplifier Characteristics

Fig. 5(a) and (b) shows the normalized maximum switch voltage V_{Smax}^* and current I_{Smax}^* as functions of duty ratio D and normalized shunt capacitance γ_S. The V_{Smax}^* and I_{Smax}^* are obtained by computing the maximum value against θ using (12) and (9), respectively. It is seen from Fig. 5(a) that the normalized peak switch voltage decreases for lower D. Meanwhile, the low switch-current stress is attained for larger γ_S, as shown in Fig. 5(b).

Fig. 5(c) shows the power-output capability, which is defined as

$$c_p = \frac{\rho {I_m^*}^2}{2 V_{\text{Smax}}^* I_{\text{Smax}}^*}. \tag{25}$$

It is seen from Fig. 5(c) that the maximum power-output capability $c_p = 0.102$ is obtained for $D = 0.481$ and $\gamma_S = 1.08$.

Fig. 6 shows the normalized extra-inductance λ_b and output current amplitude I_m^* as functions of duty ratio for fixed

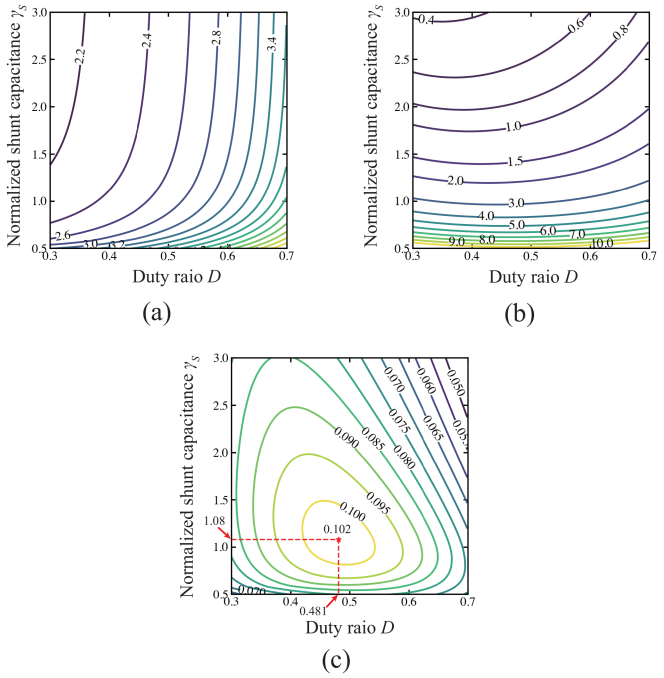

Fig. 5. Amplifier characteristics as functions of duty ratio D and normalized shunt capacitance γ_S. (a) Switch-voltage stress V^*_{Smax}. (b) Switch-current stress I^*_{Smax}. (c) Power-output capability.

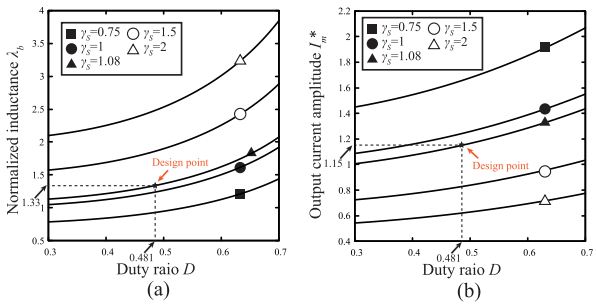

Fig. 6. Design curves of the proposed amplifier as functions of duty ratio D. (a) Normalized inductance λ_b. (b) Normalized output-current amplitude I^*_m.

γ_S, which is depicted using (23) and (24). It can be seen from Fig. 6(b) that the output current amplitude is adjustable depending on D and γ_S. The design point that achieves the maximum power-output capability is obtained as $\lambda_b = 1.33$ and $I^*_m = 1.15$.

F. Cricuit Design for Maximum Power-Output Capability

The proposed amplifier is designed for given input voltage V_I, rated load resistance R_r, switching frequency f, and quality factor Q. The component values can be uniquely determined by satisfying (18), (20), (21), (23), and (24) for any D and γ_S. The design equations for any D and γ_S, and the specific case of maximum power-output capability are derived as

$$C_S = \frac{1}{\omega\gamma_S R_r} = \frac{0.147}{fR_r} \tag{26}$$

$$L_S = \frac{1}{\omega_S^{*2} C_S} = \frac{0.0977 \times R_r}{f} \tag{27}$$

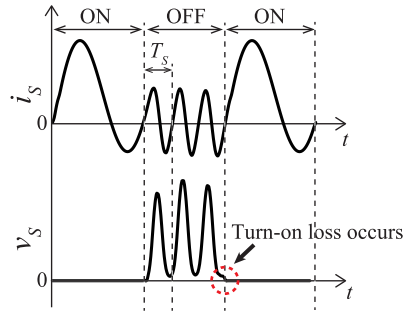

Fig. 7. Example waveforms of switch current and voltage of the proposed amplifier.

$$L_0 = \frac{QR_r}{\omega} = \frac{0.159 \times QR_r}{f} \tag{28}$$

$$L_b = \frac{\gamma_S \omega_S^{*2} R_r}{\pi\omega(\omega_S^{*2}-1)}\left\{\pi(1-D) + \frac{\sin(\pi D)}{2} - \frac{\pi}{\omega_S^{*2}} + \frac{2\sin(\pi D)\left[\sin(\pi D) + \pi(1-D)\cos(\pi D)\right]}{\pi(1-D)(\omega_S^{*2}-1)}\right\}$$

$$= \frac{0.212 \times R_r}{f} \tag{29}$$

and

$$C_0 = \frac{1}{\omega^2(L_0 - L_b)} = \frac{0.159}{fR_r(Q-1.33)}. \tag{30}$$

The amplitude of the output current is derived from (23) as

$$I_m = \frac{\pi(\omega_S^{*2}-1)V_I}{\gamma_S\omega_S^{*2}R_r[\pi(1-D)\cos(\pi D) + \sin(\pi D)]} = \frac{1.15 \times V_I}{R_r}. \tag{31}$$

G. Circuit Design for Reducing Switching Loss

The proposed amplifier achieves ZCS regardless of the load resistance, reducing the current-related turn-OFF losses. However, in high-frequency operations, voltage-related turn-ON losses become dominant. Therefore, design methods to reduce turn-ON losses is provided in this section.

The turn-ON switching loss can be given as

$$P_{\mathrm{SW}} = \frac{1}{2} C_{\mathrm{OSS}} V_S^2 f \tag{32}$$

where C_{OSS} is the output capacitance of the switching device, and V_S is the switch voltage at turn-ON instant. We can see from (32) that reducing V_S is effective for suppressing the turn-ON loss.

Fig. 7 shows the example waveforms of the switch current and voltage. There are ringings in both switch current and voltage during the turn-OFFperiod, which is caused by the resonance between L_S and C_{OSS}. For reducing V_S, it is desirable to turn ON the switch when the switch voltage drops completely, as shown in Fig. 7. Namely, the number of the ringings during the turn-OFF period should be an integer multiple as

$$n_S T_S = \frac{1-D}{f} \tag{33}$$

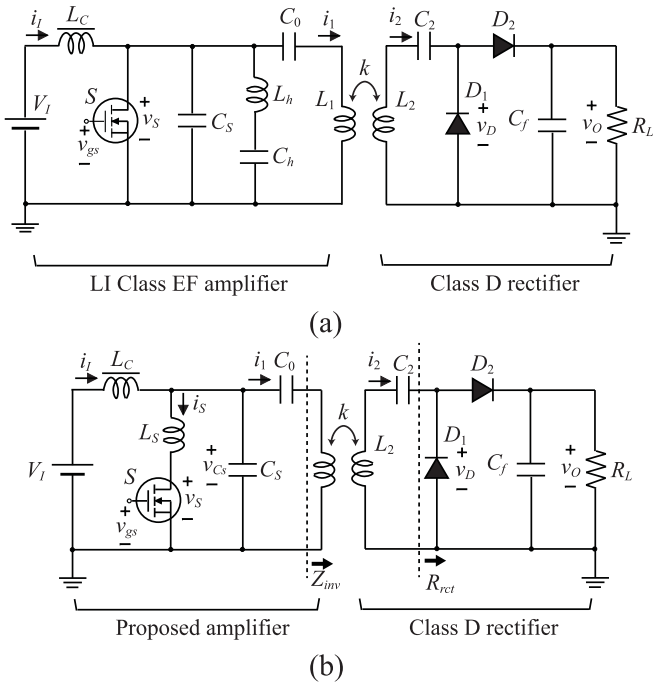

Fig. 8. Circuit configurations of the WPT system. (a) With the LI Class EF amplifier. (b) With the proposed amplifier.

where n_S is the number of the ringings, for example, $n_S = 3$ in Fig. 7. Besides, $T_S = 2\pi\sqrt{L_S C_{\rm OSS}}$ represents a ringing period. From (33), the design value of the L_S can be obtained as

$$L_S = \frac{1}{C_{\rm OSS}}\left(\frac{1-D}{\omega n_S}\right)^2. \tag{34}$$

The design equation of C_S can be

$$C_S = \frac{1}{\omega_S^{*2} L_S}. \tag{35}$$

The remaining component values can be determined using (28)–(30).

IV. Application for WPT

This article introduces a WPT system using the proposed amplifier as a concrete application example, along with a design procedure, power-loss analysis, and experiment. Furthermore, this article compares the performances of the proposed WPT system and the WPT system using the LI Class EF amplifier [15].

A. System Configuration

Fig. 8 shows the circuit configurations of the WPT system with the LI Class EF and the proposed amplifiers, respectively. The LI Class EF and the proposed amplifiers are employed as transmitters. The current-driven Class D rectifier [29] is adopted for the receiver. The Class D rectifier consists of two diodes D_1 and D_2 with parasitic capacitances of C_{D1} and C_{D2}, respectively, smoothing capacitor C_f, and load resistance R_L. The coupling section is of the series-to-series (S-S) type, and the transmitter coil L_1 and receiver coil L_2 are coupled with a coupling coefficient k.

B. Analytical Expressions of Proposed WPT System

The input impedance of the Class D rectifier is ideally pure resistive component [30]. However, in a high-frequency region, it becomes capacitive due to the parasitic capacitances of the diodes. When the parasitic capacitances C_{D1} and C_{D2} are considered, the input resistance and capacitance of the Class D rectifier can be expressed as [31]

$$R_{\rm rct} = \frac{[1-\cos(2\pi D_{\rm rct})]^2 R_L}{2\pi^2} \tag{36}$$

and

$$C_{\rm rct} = \frac{2\pi(C_{D1}+C_{D2})}{\sin(4\pi D_{\rm rct}) + 2\pi(1-2D_{\rm rct})} \tag{37}$$

respectively, where

$$D_{\rm rct} = \frac{1}{2\pi}\cos^{-1}\left[\frac{\omega(C_{D1}+C_{D2})R_L - 2\pi}{\omega(C_{D1}+C_{D2})R_L + 2\pi}\right] \tag{38}$$

is the diode ON-duty ratio.

The impedance seen from the amplifier is obtained as

$$Z_{\rm inv} = \frac{\omega^2 k^2 L_1 L_2 R_{\rm rct}}{R_{\rm rct}^2 + \frac{1}{\omega^2 C_{\rm rct}^2}} + j\omega\left[L_1 + \frac{k^2 L_1 L_2}{C_{\rm rct}\left(R_{\rm rct}^2 + \frac{1}{\omega^2 C_{\rm rct}^2}\right)}\right] \tag{39}$$

under the complete resonance in the secondary side as

$$\frac{1}{\omega\sqrt{L_2 C_2}} = 1. \tag{40}$$

It can be seen from (39) that both the resistive and reactive parts depend on the load resistance R_L. Meanwhile, the proposed amplifier has robustness even against reactive-component variations due to the low-Q SR filter.

From (39), the dc-output voltage of the WPT system with the proposed amplifier is expressed as

$$V_O = \omega k I_m \sqrt{\frac{L_1 L_2 R_{\rm rct} R_L}{2\left(R_{\rm rct}^2 + \frac{1}{\omega^2 C_{\rm rct}^2}\right)}}. \tag{41}$$

We can see from (41) that the output voltage depends on the load resistance R_L. When we consider the case that the effect of the parasitic capacitance of the diode can be ignored, namely, $R_{\rm rct} \gg 1/(\omega C_{\rm rct})$, the output voltage is derived from (31) and (41) as

$$V_O = \frac{\pi k \omega \sqrt{L_1 L_2}}{2} I_m = \frac{0.0677 \times R_{Lr} V_I}{k f \sqrt{L_1 L_2}}. \tag{42}$$

The parameter R_{Lr} in (42) represents the rated load resistance, which is the fixed value and is given as a design specification. Although the output voltage V_O depends on the initial design value of the load resistance R_{Lr}, the output voltage keeps a constant value against the changes in the load resistance R_L.

V. Experimental Results

The circuit experiment was conducted for the WPT system with the LI Class EF and the proposed amplifiers, shown in Fig. 8(a) and (b).

TABLE I
GEOMETRIC PARAMETERS OF TRANSMITTER AND RECEIVER COILS

	h_{core}	d_{core}	N	d_w
Transmitter coil	15 mm	60 mm	6	1.2 mm
Receiver coil	12 mm		6	1.2 mm

TABLE II
ANALYTICAL AND MEASURED COMPONENT VALUES OF THE WPT SYSTEMS

LI Class EF WPT system			WPT system with proposed amplifier		
	Analytical	Experiment		Analytical	Experiment
L_C	-	150 μH	L_C	-	150 μH
L_h	7.07 μH	7.04 μH	L_S	2.42 μH	2.42 μH
C_S	147 pF	100 pF	C_S	519 pF	519 pF
C_0	20.4 nF	19.8 nF	C_0	-	1.0 μF
C_h	112 pF	111 pF	C_2	372 pF	371 pF
C_2	372 pF	371 pF	C_f	-	1.0 μF
C_f	-	1.0 μF	r_{L_C}	-	100 mΩ
r_{L_C}	-	100 mΩ	r_{L_S}	-	178 mΩ
r_{L_h}	-	304 mΩ			

A. Experimental Prototype

The design specification of the WPT system with the proposed amplifier was given as: $f = 3.39$ MHz, $V_I = 120$ V, $R_{Lr} = 50\,\Omega$, and $V_O = 65$ V. The coupling coils were solenoid-type and made with air core, having a transmission distance of $d = 15$ mm. The geometric parameters of the coupling coils are given in Table I, where h_{core} and d_{core} are the height and diameter of the coils, respectively. In addition, the turn numbers N and wire diameters d_w in Table I are determined to obtain the desired output voltage from (42).

The implemented coupling coils had inductances of $L_1 = 5.24$ μH and $L_2 = 5.93$ μH with ESRs of $r_{L_1} = 0.342$ Ω and $r_{L_2} = 0.488\,\Omega$, respectively. Besides, a measured coupling coefficient between L_1 and L_2 was $k = 0.224$. From the measured parameters, the equivalent resistance $R_{\text{inv}} = 56.5\,\Omega$ was obtained. The proposed amplifier can provide a sinusoidal output current even without the SR filter. Therefore, we used sufficiently large capacitance for C_0, which only works as a dc blocking. Table II gives the component values of the WPT system with proposed and LI Class EF amplifiers, which were obtained by following the design in Sections III-F and III-G.

The WPT system with the LI Class EF amplifier shown in Fig. 8(a) was also designed with the same coupling coils and the receiver circuit as the proposed WPT system. However, there is a difference in the voltage gain between the LI Class EF and the proposed amplifiers. Therefore, the input voltage of the WPT system with the LI Class EF amplifier was set to $V_I = 180$ V to obtain the same output voltage as the proposed WPT system. Table II gives the component values of the WPT system with the LI Class EF amplifier, which were designed with the ON-duty ratio of $D = 0.3$ [15].

For implementing the WPT system, we selected GS-065-004-1-L GaN E-HEMT from GaN Systems for the switching device, whose ON-resistance was $r_S = 0.45\,\Omega$. Fig. 9 shows the output capacitance of the selected GaN E-HEMT as a function of the switch voltage. It is essential for the proposed amplifier to select the switching device whose output capacitance is sufficiently low. This is because the analysis given in Section III does not consider the output capacitance. The T68-6 iron-powder toroidal core from Micrometals was used to implement the series inductance L_S. The STPS5H100 Schottky Rectifier from STMicroelectronics was adopted for the diode D_1 and D_2, whose ON-resistance, forward voltage, and parasitic capacitance were $0.024\,\Omega$, 0.49 V, and 90 pF, respectively. The experimental component values are given in Table II, which were measured by E4990 A Impedance Analyzer from Keysight Technologies. Fig. 10 shows a photograph of the implemented WPT system with the proposed amplifier and the Class D rectifier.

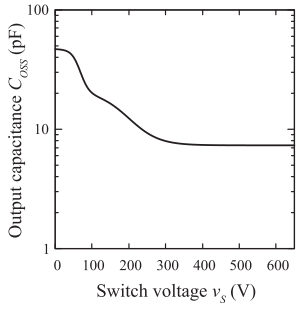

Fig. 9. Output capacitance of the selected GaN E-HEMT as a function of the switch voltage.

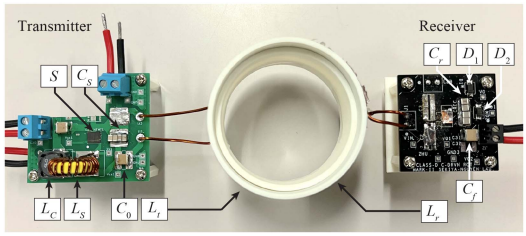

Fig. 10. Photograph of the implemented proposed WPT system.

B. Operating Waveform

Fig. 11(a)–(c) shows the experimental waveforms of the WPT system with the LI Class EF amplifier. It is seen from Fig. 11(a)–(c) that the switch voltage v_S achieved the ZVS regardless of the load resistance. In addition, the amplitude and the phase shift of the transmission current i_1 were constant even for different load resistances due to the LI design. However, the current i_1 comprises significant harmonics due to the specific tuning of the L_h-C_h for the LI design.

Fig. 11(d)–(f) shows the experimental waveforms of the WPT system with the proposed amplifier. We can see from Fig. 11(d)–(f) that the switch current i_S achieved the ZCS, and the amplitude of current i_1 was constant regardless of the load resistance. The switch voltage at the turn-ON moment was reduced, effectively suppressing the turn-ON switching loss, as described in Section III-G. Besides, the current i_1 became a sinusoidal waveform despite the absence of the SR filter. The voltage across the diode D_1 was strongly influenced by parasitic capacitance, resulting in long rise and fall times for light load conditions, as given in (38). Also, the reactance component seen from the amplifier changes with dc load variations due to the

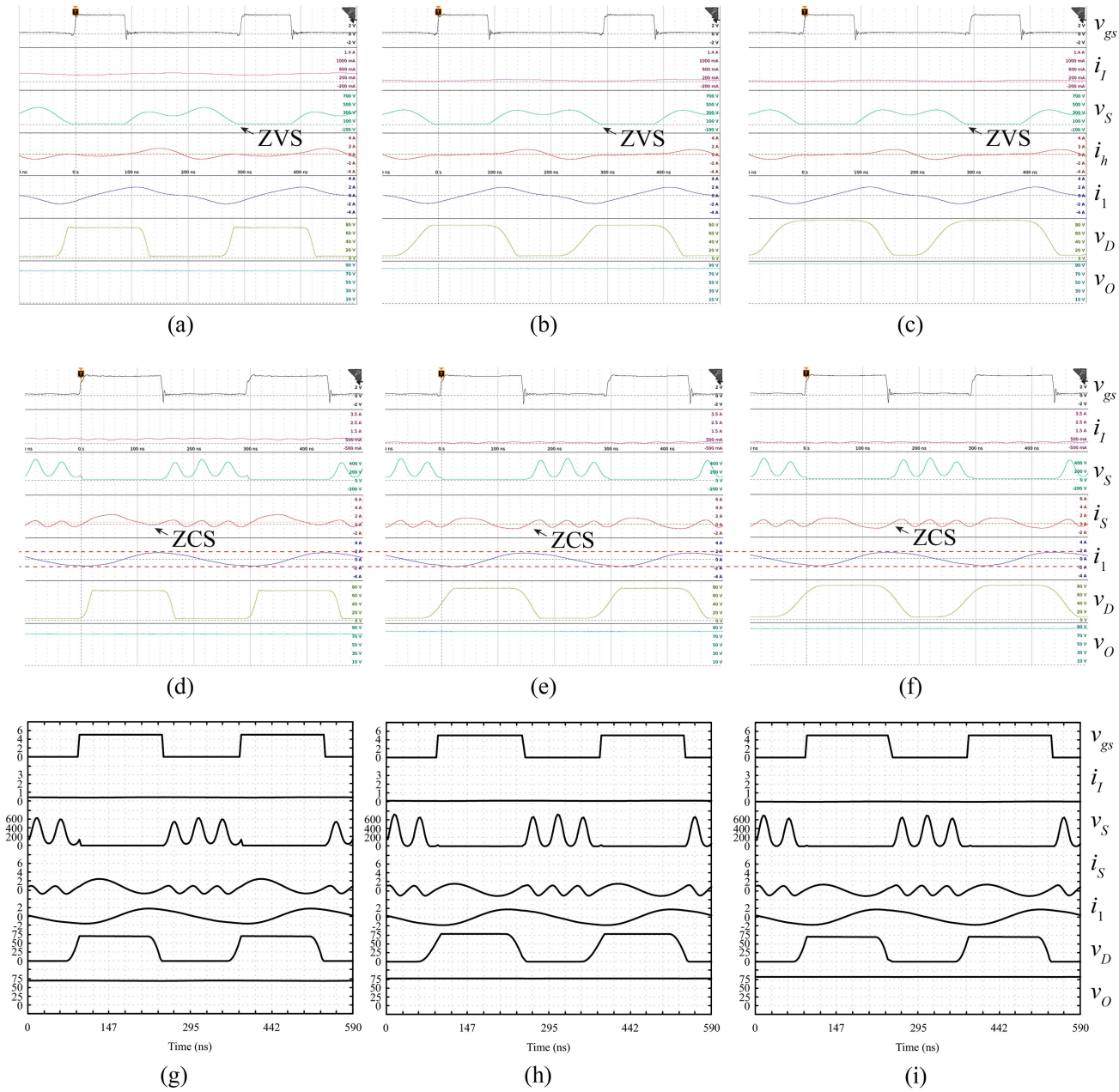

Fig. 11. Experimental and numerical waveforms of the WPT systems. (a) With the LI Class EF amplifier for $R_L = 100\,\Omega$ (Experiment). (b) With the LI Class EF amplifier for $R_L = 1\,\mathrm{k}\Omega$ (experiment). (c) With the LI Class EF amplifier for open load (Experiment). (d) With the proposed amplifier for $R_L = 100\,\Omega$ (Experiment). (e) With the proposed amplifier for $R_L = 1\,\mathrm{k}\Omega$ (Experiment). (f) With the proposed amplifier for open load. (Experiment.) (g) With the proposed amplifier for $R_L = 100\,\Omega$ (Numerical). (h) With the proposed amplifier for $R_L = 1\,\mathrm{k}\Omega$ (Numerical). (i) With the proposed amplifier for open load (Numerical).

parasitic capacitances of the diodes. Nevertheless, the proposed amplifier achieves consistent CC operation. This is because the proposed amplifier did not use the SR filter and was less sensitive against reactance component variations. These results demonstrate the effectiveness of the proposed amplifier.

Fig. 11(g)–(i) shows the numerical waveforms of the WPT system with the proposed amplifier for $R_L = 100\,\Omega$ and $R_L = 1\,\mathrm{k}\Omega$. The waveforms are derived using the numerical analysis [32], which considers parasitic components, including the nonlinear output capacitance shown in Fig. 9, the ON-resistances of the switch and diodes, and ESRs of the inductances. We can see from Fig. 11(d)–(f) and (g)–(i) that the experimental and numerical waveforms showed good agreement, which demonstrates the validity of the experimental results.

C. Circuit Characteristics

Fig. 12 shows the experimental characteristics of the WPT system with the proposed and LI Class EF amplifiers as a function of normalized load resistance. The experimental power-delivery efficiency was calculated as

$$\eta = \frac{P_O^2}{V_I I_I} \tag{43}$$

where P_O is the dc-output power.

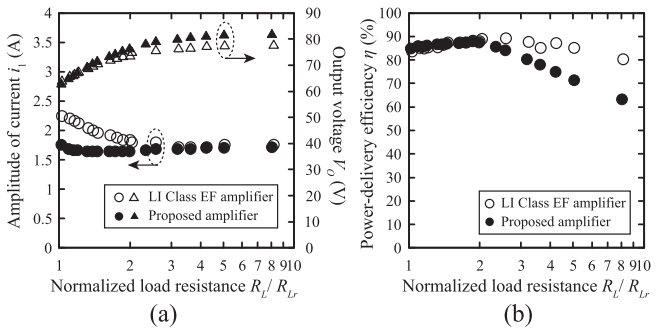

Fig. 12. Experimental characteristics of the WPT system with the LI Class EF and the proposed amplifiers as a function of normalized load resistance. (a) Amplitude of the current i_1 and output voltage V_O. (b) Power-delivery efficiency η.

We can see from Fig. 12(a) that the transmission current amplitude of the LI Class EF amplifier changed at the small load resistance. On the other hand, the proposed amplifier maintained consistent CC operation. This is because the proposed amplifier exhibits robustness even against reactive-component variations due to the low-Q output filter. Although relatively large ESRs exist in the coupling coils, they are absorbed by the equivalent resistance seen from the amplifier in the S-S coupling. Therefore, the CC operation of the proposed amplifier was not significantly affected by the ESRs.

We can see from Fig. 12(a) that the output voltage of both WPT systems increased as the load resistance. The output voltage can be constant against load variations in an ideal case where the diodes have no parasitic capacitance, as given in (42). However, the effects of the parasitic capacitances appear at high-frequency operations. As a result, the output voltage varied depending on the load resistance, as given in (41). The weak output-voltage regulation is an essential issue in the LI amplifiers [11], [12], [13], [14], [15], [16], [17], [18], [19]. Therefore, the dc–dc converter is typically added after the rectifier stage [16] for further accuracy of the output regulation. Also, the numerical design method, which can consider the parasitic components of the devices, has been proposed [33]. Although the method has a high computational cost, it is effective for the WPT system with the proposed amplifier to increase the accuracy of the output-voltage regulation.

Fig. 12(b) demonstrates that the WPT system with the proposed amplifier achieved the same level of efficiency at heavy load as the WPT system with the LI Class EF amplifier. However, the efficiency of the proposed amplifier decreased at light load. This is because the proposed amplifier had a turn-ON switching loss, which cannot be negligible at light load. The peak dc–dc efficiency 88% was achieved for 60 W output power in the proposed WPT system.

Fig. 13 shows the power-loss breakdown of the WPT system with the proposed amplifier, where the subscript of the symbol indicates the power-loss factor. The power losses are calculated by using the numerical analysis [32], which considers the ESR of inductors, on resistances of the switching device and diodes, the forward voltage of the diodes, and turn-ON switching loss as power-loss factors. We can see from Fig. 13 that the power-loss

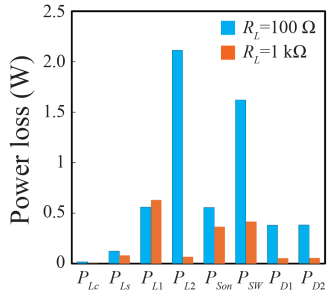

Fig. 13. Power-loss breakdown of the WPT system with the proposed amplifier for $R_L = 100\ \Omega$ and $R_L = 1$ kΩ.

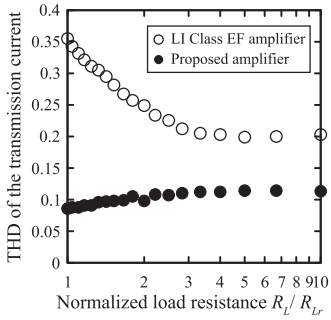

Fig. 14. THD of the output current as a function of normalized load resistance.

due to the ESR of L_2 and the turn-ON switching loss are the dominant factors at heavy load. Meanwhile, the power loss due to the ESR of L_1 becomes dominant at the light load. This is because the power loss in the transmitter coil is constant against load variations due to the CC operation, which is the major challenge for the CC amplifiers. Although CC amplifiers are naturally inefficient at light loads, they are appropriate for the transmitter of the WPT systems from the perspective of overcurrent protection. The predicted power-delivery efficiency for $R_L = 100\ \Omega$ and $R_L = 1$ kΩ are 88.3% and 41.7%, which are quantitatively agrees with the experimental efficeincy of 88.0% and 41.3%, respectively.

Fig. 14 shows the THD of transmission current i_1 in the WPT system with the Class EF and the proposed amplifiers. The THD of the transmission current is defined as

$$\mathrm{THD} = \frac{\sqrt{\sum_{n=2}^{\infty} {I^*_{mn}}^2}}{I^*_m} \tag{44}$$

where I^*_{mk} is the normalized amplitude of kth harmonic current flowing through transmitter coil. We can see from Fig. 14 that the proposed amplifier achieved lower THD than the LI Class EF amplifier over the entire load range. The THD of the LI Class EF amplifier increases, especially for the small load resistance, because the loaded quality factor of the SR filter becomes small. On the other hand, the proposed amplifier inherently outputs a sinusoidal waveform without the SR filter. Therefore, the THD of the output current is almost constant against load variations.

Based on the experimental results, we can verify that the proposed amplifier mitigated harmonic currents in the coupling part of the WPT system. Furthermore, the WPT system incorporating the proposed amplifier achieved superior consistency of the CC operation compared with the WPT system with the LI Class

TABLE III
LI AMPLIFIERS WITH CC OUTPUT FEATURE

	Aldhaher [15]	Tomohiro [14]	Huang [27]	Huang [19]	Zhu [21]	This work
Circuit topology	Class EF	Class E	Push-pull Class E	Push-pull Class Φ	Class F/E	Inverse Class E
Output resonant filter	Series	Parallel	LCCL	LCCL	Parallel	Series
Component number	6	4	7	8	5 or 7	5
Switching type	ZVS	ZVS	ZVS	ZVS	ZCS	ZCS
Output	CC	CC	CC	CC	CC	CC
Power-output capability	0.0882	0.101	-	-	0.085	0.102
Frequency (MHz)	13.56	1	6.78	6.78	1	3.39
Output power (W)	14-150	0.3-11.5	0-320	70-320	2.5-25	0-75
Efficiency	94.4% (DC/AC)	89.3% (DC/AC)	89.3% (DC/DC)	91% (DC/DC)	94.2% (DC/AC)	88.0% (DC/DC)

EF amplifier. These results substantiate the effectiveness of the proposed amplifier.

VI. COMPARISON WITH PREVIOUS WORKS

Table III gives the LI amplifiers with CC output characteristics proposed so far. The LI Class EF amplifier [15] has the SR-CC feature, which is suitable for the transmitter of the WPT system. Furthermore, the switch-voltage stress is suppressed by utilizing the harmonic resonant filter. However, the output current suffers from harmonic distortion. The LI Class E amplifier [14] achieves CC output with a PR output filter. Although the amplifier has a floating load, it consists of only four passive elements, contributing to circuit miniaturization. The LI push–pull Class E and Class Φ amplifiers [19], [27] apply the *LCCL* filter to attain the CC output. The amplifiers introduce a three-winding coupled inductor, reducing harmonics in the input current. The LI Class F/E amplifier [21] has a dual topology with the LI Class EF amplifier [15] and achieves ZCS and CC output regardless of the load resistance with the PR filter.

The proposed amplifier has the switch voltage and current waveforms, which are less sensitive against load variations compared with the original Class E amplifiers. Moreover, the proposed LI amplifier can inherently produce a purely sinusoidal output even with a low-Q output filter. Consequently, it exhibits lower sensitivity to component variations in the resonant filter. This unique characteristic represents an advantage of the proposed amplifier.

VII. CONCLUSION

This article has presented the analysis and design of the LI-SR power amplifier with CC output, along with its WPT system application. The proposed amplifier inherently achieves ZCS and a CC output regardless of the load resistance. Furthermore, the proposed amplifier can generate a sufficiently pure sinusoidal output even with a low-Q SR filter. In the experiment, the WPT system that incorporates the proposed amplifier as the transmitter was implemented. The experimental results demonstrated that the proposed amplifier achieved superior consistency of the CC operation and reduced THD of current flowing through the transmitter coil compared with the WPT system employing the LI Class EF amplifier. The experimental results showed the validity of the amplifier design and analysis.

REFERENCES

[1] X. Hao, J. Zou, K. Yin, X. Ma, and T. Dong, "Enhanced power conversion capability of class-E power amplifiers with GaN HEMT based on cross-quadrant operation," *IEEE Trans. Power Electron.*, vol. 37, no. 11, pp. 13966–13977, Nov. 2022.

[2] K. N. Surakitbovorn and J. M. Rivas-Davila, "On the optimization of a class-E power amplifier with GaN HEMTs at megahertz operation," *IEEE Trans. Power Electron.*, vol. 35, no. 4, pp. 4009–4023, Apr. 2020.

[3] Z. Tong, L. Gu, Z. Ye, K. Surakitbovorn, and J. Rivas-Davila, "On the techniques to utilize SiC power devices in high- and very high-frequency power converters," *IEEE Trans. Power Electron.*, vol. 34, no. 12, pp. 12181–12192, Dec. 2019.

[4] N. Sokal and A. Sokal, "Class E-A new class of high-efficiency tuned single-ended switching power amplifiers," *IEEE J. Solid-State Circuits*, vol. 10, no. 3, pp. 168–176, Jun. 1975.

[5] A. Ghahremani, A.-J. Annema, and B. Nauta, "Load mismatch sensitivity of class-E power amplifiers," *IEEE Trans. Microw. Theory Techn.*, vol. 67, no. 1, pp. 216–230, Jan. 2019.

[6] S. Park and J. Rivas-Davila, "Duty cycle and frequency modulations in class-E DC-DC converters for a wide range of input and output voltages," *IEEE Trans. Power Electron.*, vol. 33, no. 12, pp. 10524–10538, Dec. 2018.

[7] R. Zulinski and K. Grady, "Load-independent class E power inverters. I. Theoretical development," *IEEE Trans. Circuits Syst.*, vol. 37, no. 8, pp. 1010–1018, Aug. 1990.

[8] M. Liu, C. Zhao, J. Song, and C. Ma, "Battery charging profile-based parameter design of a 6.78-MHz class E^2 wireless charging system," *IEEE Trans. Ind. Electron.*, vol. 64, no. 8, pp. 6169–6178, Aug. 2017.

[9] Z. Sun, Y. Wang, J. Sun, Y. Guan, and D. Xu, "Design of a strong robust wireless power transfer system with wide-range output regulation based on dual-band architecture," *IEEE Trans. Ind. Electron.*, vol. 70, no. 11, pp. 11142–11152, Nov. 2023.

[10] F. Raab, "Idealized operation of the class E tuned power amplifier," *IEEE Trans. Circuits Syst.*, vol. 24, no. 12, pp. 725–735, Dec. 1977.

[11] A. Komanaka, W. Zhu, X. Wei, K. Nguyen, and H. Sekiya, "Generalized analysis of load-independent ZCS parallel-resonant inverter," *IEEE Trans. Ind. Electron.*, vol. 69, no. 1, pp. 347–356, Jan. 2022.

[12] Y. Komiyama, W. Zhu, K. Nguyen, and H. Sekiya, "Load-independent constant-current/zero-current switching inverter with series resonant filter," in *Proc. IEEE Appl. Power Electron. Conf. Expo.*, 2023, pp. 490–494.

[13] T. Sensui and H. Koizumi, "Load-independent class E^2 parallel resonant DC-DC converter," *IEEE Trans. Circuits Syst. II*, vol. 69, no. 11, pp. 4374–4378, Nov. 2022.

[14] T. Sensui and H. Koizumi, "Load-independent class E zero-voltage-switching parallel resonant inverter," *IEEE Trans. Power Electron.*, vol. 36, no. 11, pp. 12805–12818, Nov. 2021.

[15] S. Aldhaher, D. C. Yates, and P. D. Mitcheson, "Load-independent class E/EF inverters and rectifiers for MHz-switching applications," *IEEE Trans. Power Electron.*, vol. 33, no. 10, pp. 8270–8287, Oct. 2018.

[16] J. M. Arteaga, S. Aldhaher, G. Kkelis, C. Kwan, D. C. Yates, and P. D. Mitcheson, "Dynamic capabilities of multi-MHz inductive power transfer systems demonstrated with batteryless drones," *IEEE Trans. Power Electron.*, vol. 34, no. 6, pp. 5093–5104, Jun. 2019.

[17] J. M. Arteaga, S. Aldhaher, G. Kkelis, D. C. Yates, and P. D. Mitcheson, "Multi-MHz IPT systems for variable coupling," *IEEE Trans. Power Electron.*, vol. 33, no. 9, pp. 7744–7758, 2018.

[18] J. M. Rivas, O. Leitermann, Y. Han, and D. J. Perreault, "A very high frequency DC-DC converter based on a class Φ_2 resonant inverter," *IEEE Trans. Power Electron.*, vol. 26, no. 10, pp. 2980–2992, Oct. 2011.

[19] X. Huang, Y. Lin, Y. Dou, S. Lin, and J. Huang, "Load-independent push-pull class Φ_2 inverter with single compact three-winding inductor," *IEEE Trans. Power Electron.*, vol. 38, no. 10, pp. 11916–11927, Oct. 2023.
[20] H. Sekiya, K. Tokano, W. Zhu, Y. Komiyama, and K. Nguyen, "Design procedure of load-independent class-E WPT systems and its application in robot arm," *IEEE Trans. Ind. Electron.*, vol. 70, no. 10, pp. 10014–10023, Oct. 2023.
[21] W. Zhu, Y. Komiyama, A. Komanaka, K. Nguyen, and H. Sekiya, "Analysis of load-independent ZCS parallel-resonant inverter with constant current," *IEEE Trans. Ind. Electron.*, early access, Nov. 28, 2023, doi: 10.1109/TIE.2023.3333019.
[22] S. Kee, I. Aoki, A. Hajimiri, and D. Rutledge, "The class-e/f family of ZVS switching amplifiers," *IEEE Trans. Microw. Theory Tech.*, vol. 51, no. 6, pp. 1677–1690, 2003.
[23] Z. Kaczmarczyk, "High-efficiency class E, EF_2, and E/F_3 inverters," *IEEE Trans. Ind. Electron.*, vol. 53, no. 5, pp. 1584–1593, Oct. 2006.
[24] I. Nikiforidis, J. M. Arteaga, C. H. Kwan, N. Pucci, D. C. Yates, and P. D. Mitcheson, "Generalized multistage modeling and tuning algorithm for class EF and class ϕ inverters to eliminate iterative retuning," *IEEE Trans. Power Electron.*, vol. 37, no. 10, pp. 12877–12900, Oct. 2022.
[25] S. Aldhaher and P. D. Mitcheson, "500 W 13.56 MHz class EF push-pull inverter for advanced dynamic wireless power applications," in *Proc. IEEE PELS Workshop Emerg. Technol. Wireless Power Transf.*, 2019, pp. 263–267.
[26] M. Liu, M. Fu, and C. Ma, "Low-harmonic-contents and high-efficiency class E full-wave current-driven rectifier for megahertz wireless power transfer systems," *IEEE Trans. Power Electron.*, vol. 32, no. 2, pp. 1198–1209, Feb. 2017.
[27] X. Huang, Z. Yu, Y. Dou, S. Lin, Z. Ouyang, and M. A. E. Andersen, "Load-independent push-pull class E topology with coupled inductors for MHz-WPT applications," *IEEE Trans. Power Electron.*, vol. 37, no. 7, pp. 8726–8737, Jul. 2022.
[28] T. Mury and V. F. Fusco, "Inverse class-E amplifier with transmission-line harmonic suppression," *IEEE Trans. Circuits Syst. I*, vol. 54, no. 7, pp. 1555–1561, Jul. 2007.
[29] M. Kazimierczuk, "Class D current-driven rectifiers for resonant DC/DC converter applications," *IEEE Trans. Ind. Electron.*, vol. 38, no. 5, pp. 344–354, Oct. 1991.
[30] M. K. Kazimierczuk and D. Czarkowski, *Resonant Power Converters*. Hoboken, NJ, USA: Wiley, 2011.
[31] K. Fukui and H. Koizumi, "Analysis of half-wave class DE low dv/dt rectifier at any duty ratio," *IEEE Trans. Power Electron.*, vol. 29, no. 1, pp. 234–245, Jan. 2014.
[32] W. Zhu, Y. Komiyama, K. Nguyen, and H. Sekiya, "Comprehensive and simplified numerical design procedure for class-E switching circuits," *IEEE Access*, vol. 9, pp. 149971–149981, 2021.
[33] W. Zhu, Y. Komiyama, K. Nguyen, and H. Sekiya, "Heuristic algorithm-based design method for class-E switching circuits," in *Proc. IEEE Energy Conv. Congr. Expo.*, 2021, pp. 5692–5697.

Yutaro Komiyama (Graduate Student Member, IEEE) was born in Nagano, Japan. He received the B.E. and M.E. degrees in mathematics and informatics from Chiba University, Japan, in 2021 and 2022, respectively. Since 2022, he has been working toward the Ph.D. degree in mathematics and informatics with the Graduate School of Science and Engineering, Chiba University.

His research interests include high-frequency inverters and power oscillators and their application for wireless power transfer systems.

Ayano Komanaka was born in Aichi, Japan, in 1997. She received the B.E. and M.E. degrees in mathematics and informatics from Chiba University, Japan, in 2020 and 2022, respectively. Since 2023, she has been working toward the Ph.D. degree in mathematics and informatics with the Graduate School of Science and Engineering, Chiba University.

Her research interest is about high-frequency and high-efficiency inverters.

Wenqi Zhu (Member, IEEE) received the B.E. degree in electrical engineering and automation from the School of Electric Engineering and Automation, Anhui University, P. R. China, in 2016, and the M.E. and Ph.D. degrees in mathematics and informatics from Chiba University, Japan in 2020 and 2022, respectively.

He is currently a Post Doctoral Fellow in Chiba University. His current research interest is dc–dc, ac–dc power converters, and WPT systems.

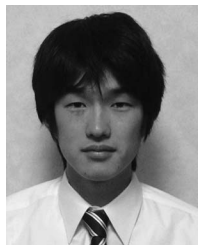

Akihiro Konishi (Member, IEEE) received the B.S. degree in electrical engineering from the Faculty of Advanced Engineering of National Institute of Technology, Nara College, Nara, Japan, in 2017, and the M.S. and Ph.D. degrees in electrical engineering from Okayama University, Okayama, Japan, in 2019 and 2023, respectively.

He is currently a Project Assistant Professor with Chiba University, Chiba, Japan.

Kien Nguyen (Senior Member, IEEE) received the B.E. degree in electronics and telecommunication from the Hanoi University of Science and Technology, Hanoi, Vietnam, in 2004, and the Ph.D. degree in informatics from the Graduate University for Advanced Studies, Hayama, Japan, in 2012.

During 2014–2018, he was a Researcher with the National Institute of Information and Communication Technology, Tokyo, Japan. Since 2018, he has been an Associate Professor with the Graduate School of Engineering, Chiba University, Chiba, Japan.

Hiroo Sekiya (Senior Member, IEEE) was born in Tokyo, Japan. He received the B.E., M.E., and Ph.D. degrees in electrical engineering from Keio University, Yokohama, Japan, in 1996, 1998, and 2001, respectively.

Since 2001, he has been with Chiba University, Chiba, Japan, where he is currently a Professor with the Graduate School of Engineering. From 2008 to 2010, he was a Visiting Scholar with the Department of Electrical Engineering, Wright State University, Dayton, OH, USA.